Int. J. Electrochem. Sci., 10 **(2015)** 1792 - 1808

International Journal of ELECTROCHEMICAL SCIENCE
www.electrochemsci.org

Corrosion Behavior of AlMgSi Alloy in Aqueous Saline Solution

R. A. Rodríguez-Diaz[1,2,*], *J. Uruchurtu-chavarín*[2], *A. M. Cotero-Villegas*[3], *S. Valdez*[4], *J. A. Juárez-Islas*[1]

[1] Instituto de Investigaciones en Materiales, Universidad Nacional Autónoma de México, Circuito Escolar S/N, Cd. Universitaria, 04510, México, D.F., México.
[2] U.A.E.M.-C.I.I.C.A.P. Av. Universidad 1001, Col. Chamilpa, 62500 - Cuernavaca, Mor., México.
[3] Facultad de Ciencias Químicas e Ingenierías, Universidad Autónoma del Estado de Morelos, Av. Universidad 1001, Chamilpa, Cuernavaca 62209, Morelos, México.
[4] Instituto de Ciencias Físicas-UNAM, Av. Universidad S/N, Col. Chamilpa, Cuernavaca, C.P. 62210, Morelos, México.
[*]E-mail: rdiaz.unam@gmail.com

Received: 19 September 2014 / *Accepted:* 29 November 2014 / *Published:* 30 December 2014

The corrosion behavior of AlMgSi alloy in a solution of 3.5 % NaCl in H_2O as a function of time of immersion has been studied and assessed by means of electrochemical techniques. These included potentiodynamic polarization curves, linear polarization resistance (LPR), electrochemical impedance spectroscopy (EIS) measurements and electrochemical noise measurements (EN). The corrosion rate expressed in terms of corrosion current density of AlMgSi alloy resulted higher than that of pure Aluminum. The precipitation of Mg_2Si phase and the formation of the galvanic couple Al-Mg induced a shift of the current density towards higher values. According to electrochemical noise measurements, the Al-based alloy experienced a localized type of corrosion at virtually all the time of exposure. The hydroxide or oxide films formed over the surface of AlMgSi alloy were not totally protective. The electrochemical behavior of corrosion has been explained in terms of the stability of the corrosion products formed film.

Keywords: Corrosion, AlMgSi alloy, Al-based alloy, Mg_2Si precipitate, Electrochemical Technique, NaCl solution.

1. INTRODUCTION

Nowadays, a number of various cast aluminum alloys have been subject to particular study and attention because of their high production, high strength and low density. Cast aluminum alloys have been utilized in various engineering applications, especially in automotive parts. In addition, aluminum alloys have also been used as the primary kind of materials for the structural parts of aircraft for more than 8 decades because of their well-known good performance, and also to the well-established design

methods, manufacturing and reliable inspection techniques [1-2]. Al-Si casting alloys have been widely used in the automotive industry, mainly due to their high castability and elevated mechanical properties. Al-Si alloys are being used for several tribological applications, such as pistons, liners, clutches, pulleys, pivots and combustion engines [3,4].

Interest in the addition of magnesium to the aluminum matrix is motivated by the application of AlMg alloys and AlMgSi in the automotive and aerospace industries due to their high mechanical strength and light weight [2]. Because of their light weight, low density, good mechanical behavior and corrosion resistance, Al-Mg-Si alloys are considered as the most used structural materials. The precipitation process that occurs in these alloys has been studied extensively because of its drastic effect on its mechanical properties [5-7].

AlMgSi alloys reach up to 90 % of the total extruded volume owing to an attractive combination of mechanical and chemical properties, also to the extrusion and an excellent response to surface finishing operations [8]. Aluminum 6000 series alloys (AlMgSi and AlMgsiCu alloys) are greatly used as extruded pieces, e.g. in automotive, marine and architectural applications [9]. However, susceptibility to intergranular corrosion (IGC) may occur as a result of inadequate thermal treatment or alloying as reported previously [10, 11].

Zahavi et al. (1982) and Ambat et al. (2006) reported that Al alloys frequently exhibit a number of troubles related to localized corrosion attack, despite the significant corrosion resistance typically obtained in these alloys which are passive in the pH domain ranging from 3 to 8 [12-13]. Besides, on behalf of the low solubility limit of alloying elements intermetallics form, which induces heterogeneities that play a significant role in the local distribution and rate of cathodic and anodic reactions. For Al-Mg-Si alloys, intermetallics and grain boundaries are seen as the main anodic corrosion initiation sites, and most of intermetallics increase the corrosion rate due to their cathodic nature [13-16]. The main intermetallics present in Al-Mg-Si alloys are Fe-containing intermetallics (noble compared to the matrix) and MgSi precipitates which possess an ambivalent electrochemical behavior.

Generally, it has been reported that the excess of Si (which induces a major precipitation of MgSi), added in Al-Mg-Si alloys mainly to obtain higher mechanical strength, leads to a greater intergranular corrosion susceptibility. The MgSi particles have shown, for various aluminum alloys, active anodic dissolution of Mg within seconds after immersion in aggressive chloride-containing solutions [17-20].

Thus, the purpose of this work is to investigate the effect of alloying with Mg and Si to the Al element on its corrosion resistance when is exposed to an aqueous saline solution, in order to expand its potential applications as structural material in the automotive, naval and aerospace industries.

2. EXPERIMENTAL PROCEDURE

2.1. Materials

The nominal chemical composition of the AlMgSi alloy was obtained by the atomic emission spectrometry technique by using an Spectrolab Lax M8-Windows equipment. The chemical composition obtained in this way, is given in Table 1.

The AlMgSi alloy was elaborated by mixing pieces of commercial elements of Al, Si and Mg (ingots with a purity of 99.8 at. %). The melting unit of alloy was of 500g, and was prepared by the high-frequency vacuum induction melting technique. The mixture of Al, Mg and Si was placed inside a silicon carbide crucible and then was melted at 760°C. In all the experiments, the molten Al-Mg-Si alloy was cast at 100°C superheat above the liquidus temperature into a cylinder shaped steel mould.

Table 1. Chemical composition of AlMgSi alloy

Elements	Al	Mg	Si
Atomic percent (%)	93.04	2.095	4.85

2.2 Sample preparation

The produced ingots were cut by a diamond wheel cutter into small cylinder pieces. Samples with an exposed area ranging from 0.5 to 1.0 cm^2 were prepared by encapsulation in epoxy resin.

For revealing the internal structure of Al-Mg alloy, the specimens were metallographically prepared prior to observation and examination by optical and electron microscopy in order to gain valuable data about AlMgSi alloy characteristics. Metallographic preparation of encapsulated specimens was performed by grinding the specimens from 400 to 2000 grit paper and polished with 1 µm alumina powder.

2.3. Electrochemical Techniques.

For the corrosion tests, a 3.5% NaCl solution was used at room temperature (≈ 25 °C). Potentiodynamic polarization curves were obtained by varying the applied potential from (–2000 mV) with respect to the free corrosion potential, E_{corr}, up to 0.0 mV at a scan rate of (1 mV/s). A conventional three electrodes glass cell was used with a graphite rod as auxiliary electrode and a saturated calomel electrode (SCE) as reference. Corrosion current density values, I_{corr}, were calculated by using the Tafel extrapolation method and by taking an extrapolation interval of ± 250 mV around the E_{corr} value once stable. Linear polarization resistance, LPR, measurements were carried out by polarizing the specimen from +10 to – 10 mV with respect to E_{corr}, at a scanning rate of 1 mV/s periodically within the total immersion time of 30 days. Electrochemical impedance spectroscopy tests were carried out at E_{corr} by using an AC signal with amplitude of ±20 mV and a frequency interval of 0.05 Hz – 10 kHz. The electrochemical free corrosion potential as a function of time of the working electrodes Ecorr, was measured versus a saturated calomel reference electrode (SCE). Electrochemical noise measurements (EN) in both current and potential were recorded using two *identical* working electrodes and a reference electrode (SCE). The electrochemical noise measurements were made recording simultaneously the potential and current fluctuations at a sampling rate of one point per

second for a period of 1024 seconds. Removal of the DC trend from the raw noise data was the first step in the noise analysis when needed. To accomplish this, a least square fitting method was used.

An ACM potentiostat controlled by a desktop computer was used for all the electrochemical tests. The linear polarization resistance, electrochemical impedance spectroscopy and electrochemical noise measurements, were performed during different days within a period of 15 days.

2.4 Microstructural analysis of as-cast and corroded specimens.

The as-cast specimen was encapsulated in epoxy resin and the metallographic preparation of the encapsulated specimen was performed by grinding the sample from 400 to 2000 grit paper and polished with 1 μm alumina slurry. The as-cast specimen surface was analyzed with a scanning electron microscope (SEM) with an accelerating voltage of 25 keV. Chemical microanalysis and X-ray chemical mapping were carried out with an energy dispersive X-ray analyzer (EDX) attached to the SEM.

In order to determine the crystal structure and phases identification in the corrosion products, a Siemens 5000 X-ray diffractometer was employed, using Cu tube (Kα line radiation: $\lambda = 0.15406$ nm), and a diffracting beam graphite monochromator. The XRD patterns were recorded in the 2θ range from 5° to 120° (with step size 0.02, time per step 0.6 s).

3. RESULTS AND DISCUSSION.

In order to explain the nature of the Al-Mg alloy plus its inherent properties and the ability of being processed by a traditional casting process with cost-effective use, we need to analyze their internal structure. In addition, we have characterized the Al-Mg alloy by electrochemical methods, in order to know better the properties of the alloy and then we can be able to select the material properly for a particular application. To provide a wide range of properties, we must know various electrochemical and microstructural properties to figure out new emerging uses that could provide the Al-Mg alloy in order to surpass the competition in demanding automotive applications.

3.1 Microstructural characterization of uncorroded AlMgSi alloy by scanning electron microscopy.

The microstructure of the as-cast AlMgSi alloy is shown in Figure 1a), this micrograph exhibits an inter-dendritic region. It Is well know, that microstructure is strongly dependent of solidification process, especially by the solidification rate.

The observations by electron microscopy and chemical analyses using the EDS technique revealed that Mg and Si precipitate to a higher extent in the inter-dendritic region.

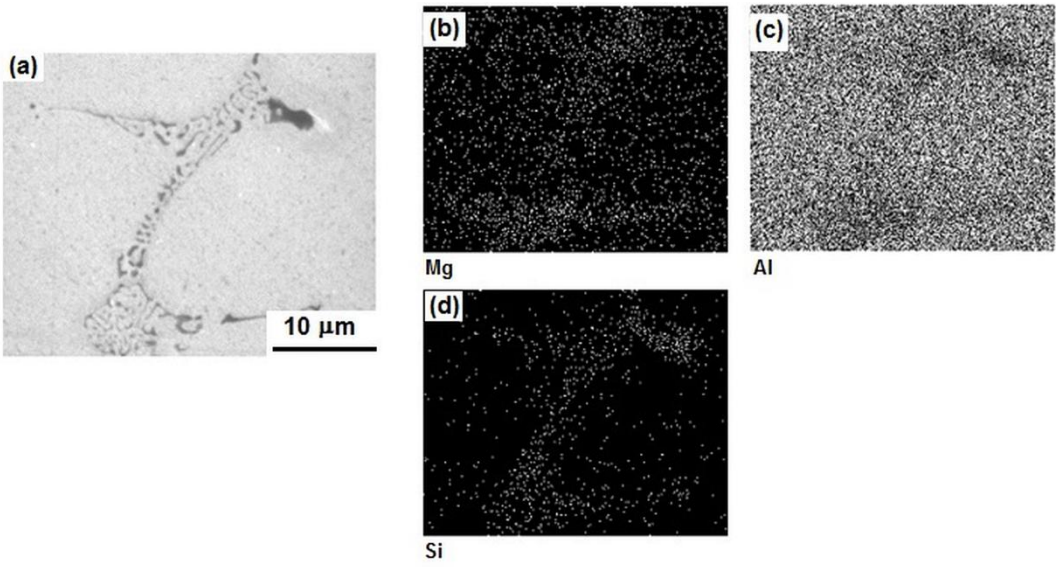

Figure 1. (a) Photomicrograph of un-corroded AlMgSi alloy together with X-ray mappings of (b) Mg, (c) Al and (d) Si.

Also, a uniform distribution of Mg in the Al matrix is observed in the X-ray mapping of Mg displayed in Figure 1b. In contrast, Si element was concentrated preferentially in the inter-dendritic spacing as shown in Figure 1d. According to the Al-Mg-Si ternary alloy phase diagram [21], in the aluminum rich corner, the Mg and Si act as solute elements and form a solid solution in the Al solvent matrix at a specific extent, forming a possible galvanic coupling site. When the concentration of Mg and Si exceed the limit of solid solubility in Al, then the Mg_2Si phase is precipitated together with a lower concentration of Si.

3.2. Potentiodynamic polarization curves.

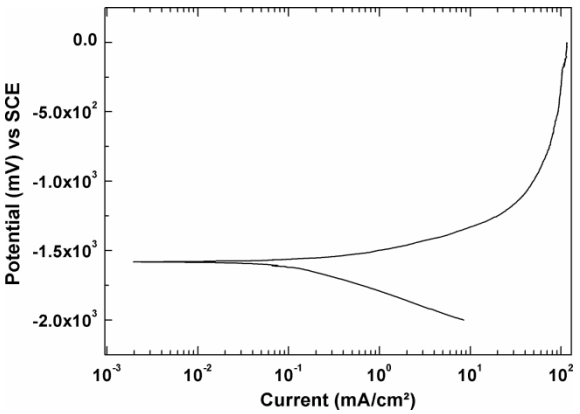

Figure 2. Polarization curve of AlMgSi alloy exposed to a 3.5% NaCl aqueous solution.

Polarization curve for AlMgSi alloy is shown in Figure 2. The ternary Al based alloy displays an active behavior only, with an E_{corr} value close to −1580 mV and a corrosion rate expressed in terms

of the I_{corr} value of the order of 0.1 mA/cm^2. For the ternary AlMgSi alloy a depolarizing region with fast dissolution in the anodic branch can be observed with the possible formation of corrosion products, reaching an anodic limit current region at higher over-potentials of about -800 mV.

Polarization curve exhibit Tafel behavior in both anodic and cathodic branches. It is worth noticing that the actual E_{corr} value presented in table 2 is more active than the corrosion potential for pure Al (-876 mV) as reported by Zeng et al. [22]. In that work, it was studied the electrochemical and coupling behavior of the single Mg_2Si and Si phases with α(Al) in a saline 3.5 % NaCl solution.

The lower E_{corr} value observed in Figure 2 can be explained in terms of the Mg, Si and Mg_2Si precipitates typically formed in AlMgSi alloys. Since the E_{corr} of the single Mg_2Si phase measured and reported by Zeng et al, (2011) resulted equal to -1159 mV in the same corrosion testing conditions. Thus in this case, the corrosion potential of Mg_2Si phase is more negative than the observed in pure (Al). This indicates that the E_{corr} value of AlMgSi alloy reported in the present research was shifted towards more negative values due to the contribution of the more negative corrosion potential of Mg_2Si phase. These findings indicate that Mg_2Si particles are more susceptible to corrosion than pure Aluminum or Si particles at the beginning of the corrosion test. It can also be asseverated that the Mg_2Si phase is anodic to the Al base alloy and corrosion occurs on its surface at the beginning.

Regarding to corrosion rate expressed in terms of current density, the AlMgSi alloy exhibited a value near to 4 x 10^{-4} A/cm^2, which is bigger than the current density

(I_{corr}) registered for pure Aluminum (I_{corr}= 7.67 x 10^{-7} A/cm^2) under the same experimental corrosion test conditions as reported previously [22]. Similarly, this behavior could be due to the fact that the current density of Mg_2Si phase is 1.28 x 10^{-6}, which is bigger than the I_{corr} for pure Al just as it was reported by Zeng et.al. Therefore the current density of Mg_2Si phase induced a shift of the overall I_{corr} value of AlMgSi alloy towards higher values. Another factor that could have contributed to raise the corrosion rate of AlMgSi alloy is the higher reactivity of Mg precipitated in the inter-dendritic regions as compared with Al and Si, forming in this way a reactive galvanic couple site. The preferential chemical degradation that underwent the Mg element can be evidenced by looking at the revealed corrosion products included in the X-ray diffraction profile displayed in figure 13. Besides, this behavior can also be due to the lower standard redox potential of Mg as compared with those of Al and Si. Therefore, the union of magnesium and aluminum resulted in the formation of a galvanic couple, wherein the Mg acted as anode, and the galvanic couple resulted in an increase of the corrosion rate of AlMgSi alloy.

The heterogeneities present at the surface of Al-based alloys include precipitates and constituent particles (intermetallic particles formed by alloying and impurity elements). At these sites micro-flaws in the aluminum oxide (Al_2O_3) film possibly exist, and there are potential differences between the particles and the aluminum matrix. The micro-flaws and the galvanic couples Al-Mg are responsible for not only the nucleation but also the growth of pits, when the alloy is exposed to an aggressive saline electrolyte.

Table 2. Electrochemical parameters obtained from polarization curves of AlMgSi alloy polarized in the saline 3.5M solution.

Alloy	E_{corr}(mV)	I_{corr}(mA/cm^2)	a_{catod} (mv/decade)	b_{anod} (mv/decade)
AlMgSi	-1580.9	0.1	211	77

3.3. E_{corr} Measurements

Figure 3 displays the change in the Potential values as a function of time for the Al-based alloy exposed to the saline solution at room temperature. It is clearly observed that the corrosion potential becomes nobler as the immersion time elapsed up to 12 days of exposure. This behavior is because as Mg is easily oxidized since a thick hydroxide film is formed when it is in contact with humid air or immersed in water [23, 24]. However, after 12 days of immersion the E_{corr} turned slightly more active (more negative) again. This behavior should be related with the formation of hydroxide film with partial protectiveness on the surface of AlMgSi alloy [23, 25, 27]. This asseveration is based on the formation of magnesium hydroxide and hydrated magnesium chloride, these phases were revealed by XRD technique, see figure 13.

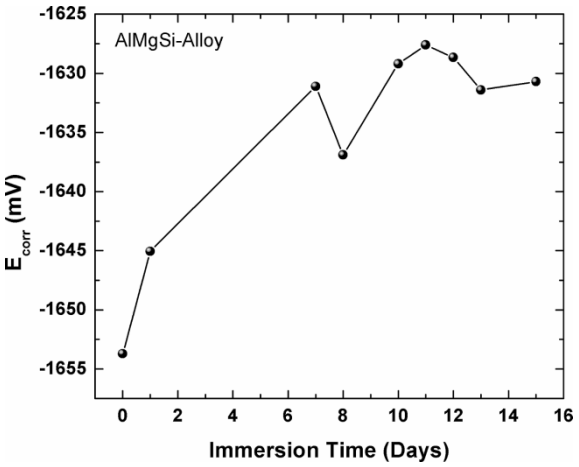

Figure 3. Variation of E_{corr} of AlMgSi alloy as a function of immersion time in 3.5 % NaCl saline aqueous solution.

3.4. R_p Measurements

The dependence of the R_p values with the exposure time for AlMgSi alloy exhibited a drastic drop from about 500 to 3 Ohm-cm^2 at the start of the time of immersion one day after, as shown in Figure 4. This behavior is due to the high reactivity and to the poor corrosion resistance of the alloy together with the fact that the pitting corrosion will occur at the free corrosion potential of magnesium and/or aluminium when exposed to chloride ions in a non-oxidizing medium [24]. Besides, as is shown in the polarization curve of the AlMgSi alloy exposed to 3.5 % NaCl solution (Figure 2), the precipitation of Mg_2Si phase turned the AlMgSi alloy more anodic. However, the R_p value increased

from 3 Ohm.cm^2 at the start of exposure to 174 (ohm.cm^2) at the 10th of immersion day in the 3.5 NaCl aqueous solution, coinciding with the corrosion potential dynamic behavior and the polarization curve, as expected. This behavior could be ascribed to the formation of a film of corrosion products on the surface of AlMgSi alloy composed by a mixture of Magnesium hydroxide, Magnesium chloride hydroxide, together with a minor content of SiO_2 as revealed in the X-ray diffraction pattern presented and displayed, later in this work. In addition, when the immersion time elapsed from the 10th to the 13th day, the R_p values decreased from 174 to 57 Ohm.cm^2; but after that, the R_p values remained more or less constant. This is due to the fact that the hydroxide or oxide films forming over the surface of AlMgSi alloy are not being perfect and protective [25].

3.5 Impedance Measurements.

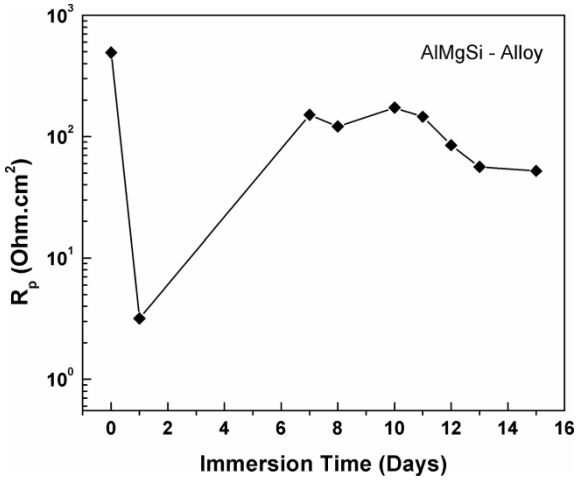

Figure 4. Variation of R_p of AlMgSi alloy as a function of immersion time in 3.5 % NaCl saline solution.

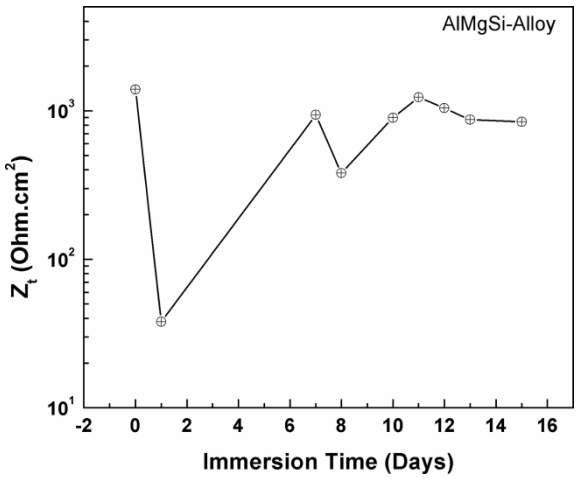

Figure 5. Variation of Z_t of AlMgSi alloy as a function of immersion time in 3.5 % NaCl saline solution.

Figure 5 displays the change in the total impedance, Z_t, with immersion time for AlMgSi alloy exposed during various days to the saline solution of 3.5 % at. in H_2O at room temperature. This plot exhibits a very similar trend to the graph of the variation of R_p as a function of immersion time, seen in Figure 4. Similarly, this behavior is due to the fact that the compounds $Mg(OH)_2$ and $Mg_{10}Cl_2(OH)_{18}$ formed over the surface of AlMgSi alloy are soluble, therefore not being very protective.

3.6 Electrochemical noise measurements

To have an insight of the susceptibility that the AlMgSi alloy could show any kind of localized corrosion such as: galvanic, pitting or intergranular attack. Various electrochemical current and potential noise tests were performed. Examples of electrochemical noise-time series in current and potential, for the AlMgSi alloy immersed in the chloride solution are presented in figures 6 to 8.

It can be seen that at the start of immersion the noise times series present stochastic behavior for the noise potential, and the noise current showed anodic and cathodic transients with moderate frequency and a relatively high intensity. This behavior suggests that this material is corroding locally at the beginning of immersion, probably due to galvanic effects and any film over the surface is broken down, and the underlying bare metal alloy corrodes locally, showing an increase in the noise current transients. Once the film layer is re-formed, this parameter decreases. Thus, these transients observed represent events of film rupture and reformation of the oxide/hydroxide layer; e.g. localized attack initiation.

When the time had elapsed to 8 days of immersion (see figure 7), both the intensity and frequency of these transients decreased, indicating a lower pitting or localized attack susceptibility of the alloy, which can be related to the growing thickness of the metal formed layer composed by a mixture of magnesium hydroxide and SiO_2 phases. As the elapsed time of immersion advanced from 8 to 15 days of exposure, the frequency of transients kept more or less constant, but the intensity of transients increased significantly, as seen in figure 8. This behavior indicates a higher pitting susceptibility of the AlMgSi alloy which is related to the imperfect protective nature of the $Mg(OH)_2$ and/or MgOHCl formed over the alloy surface.

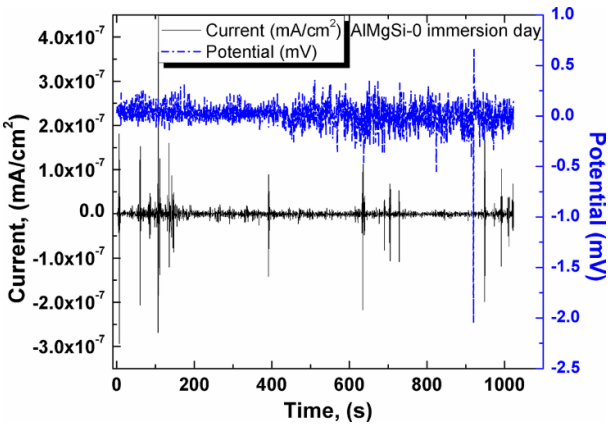

Figure 6. Electrochemical noise for AlMgSi alloy during the 0th immersion day in a 3.5 % NaCl saline solution.

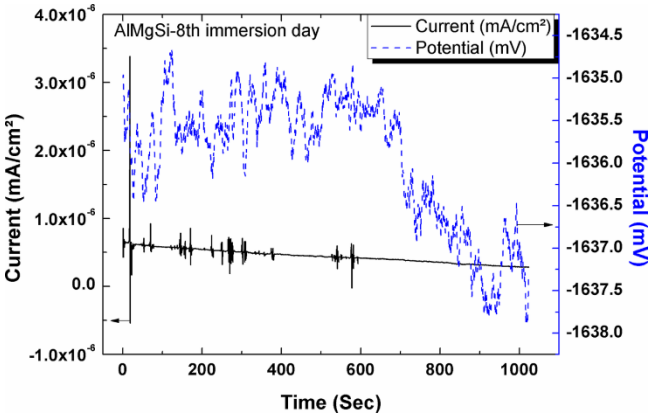

Figure 7. Electrochemical noise for AlMgSi alloy during the 8th immersion day in a 3.5 % NaCl saline solution.

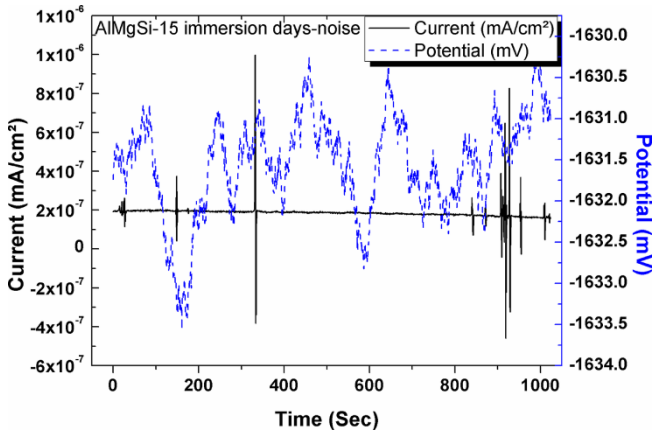

Figure 8. Electrochemical noise for AlMgSi alloy during the 15th immersion day in a 3.5 % NaCl saline solution.

When using the standard deviation of the noise potential, σ_v, and dividing it by the standard deviation of the noise current, σ_i, the noise resistance, R_n can be obtained. Figure 9 shows the variation of noise resistance with time for AlMgSi alloy.

The dependence of the R_n values with the exposure time for AlMgSi alloy exhibited a significant drop from about 5.5 x 10^6 to about 3 x 10^6 Ohm.cm^2, when the immersion time had elapsed seven days, see Figure 9. This behavior is due to the decrease of the resistance to localized pitting corrosion of the magnesium hydroxide film formed over surface of AlMgSi alloy; besides, this behavior is probably due in part to the relative high solubility of this compound in the H_20 from the solution.

However, the R_n value increased from 3x10^6 Ohm.cm^2 at the seventh day of exposure to 2x10^8 Ohm.cm^2 at the 10th day of immersion in the 3.5 NaCl aqueous solution. This behavior could be ascribed to the re-establishment of the magnesium hydroxide film together with the formation of the inert and passive SiO_2 oxide as revealed in the X-ray diffraction pattern presented, see below. In addition, when the immersion time elapsed from the 10th to the 12th day, the R_n values decreased from 2x10^8 to 8x10^6 Ohm.cm^2; but after that, the R_p values remained more or less constant.

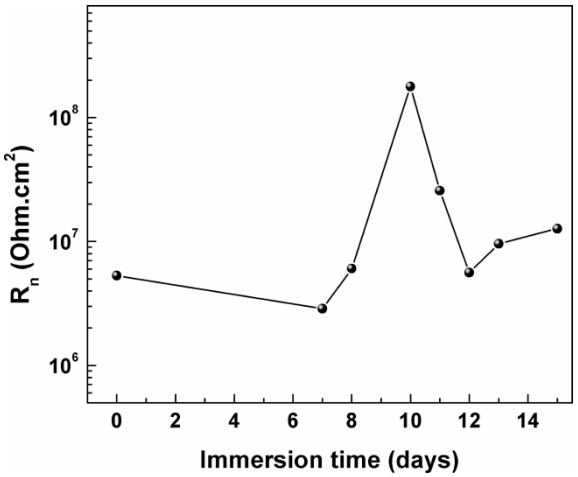

Figure 9. Variation of the noise resistance R_n of AlMgSi alloy as a function of immersion time in 3.5 % NaCl saline solution.

The overall R_n behavior observed reflects the presence of the film formed over the metal surface and the localized attack, as the main form of metal corrosion occurring over it. There is a factor called

" Localization Index, IL", defined as:

$$IL = \frac{\sigma_i}{i_{rms}} \quad (1)$$

Where σ_i is the standard deviation of the noise current and i_{rms}, the root mean squared of the noise current. Equation 1 establishes that for IL values between 1 and 0.1, the material undergoes a localized corrosion type. When the IL value is between 0.1 and 0.01, there is a mixture of both types of corrosion, localized and general. Finally, for IL values between 0.01 and 0.001, there is a tendency towards a type of uniform corrosion or passive conditions. Table 3 shows the IL values that were determined from the time series of the electrochemical noise in current of AlMgSi alloy exposed to 3.5% NaCl aqueous solution at different times of immersion. It can be concluded from table 3, that the AlMgSi alloy underwent a localized type of corrosion, during almost all the time of exposure, but with exception of the tenth day of immersion, where the Al-based alloy experienced mixed corrosion, localized and general.

In addition, aluminum alloys typically undergo localized corrosion, as a result of the highly protective aluminum oxide film which forms on the general surface and the presence of secondary phase particles (e.g., Mg_2Si precipitates formed in AlMgSi alloy). Pitting corrosion is considered to be one of the principal mechanisms for degradation of Al alloys strengthened by intermetallic precipitates.

Table 3. Localization index, "LI", determined from the time series of the electrochemical noise in current

Immersion time (days)	Localization index, LI
0	1.0
7	0.344
8	0.273
10	0.077
11	0.903
12	0.917
13	0.495
15	0.250

3.7. EIS measurements.

The corrosion behaviour of the AlMgSi alloy specimen was examined using EIS as a function of immersion time in 3.5% NaCl solution. The impedance data obtained for Al-based alloy over different periods are displayed in Figures 10, 11 and 12 in the form of both Nyquist and Bode plots.

The Bode impedance diagram shows flat regions at high and two slopes at mid and low frequencies, corresponding to the solution resistance at high frequency and the charge transfer resistance at low frequency, see Figure 10. The slopes corresponds to the film and double layer capacitances and relates to one or two RC time constant.

Quasi-inductive components in the low frequency region were observed in the AlMgSi alloy, at all exposure times, better observed in the EIS Nyquist plots reflected in a second peak in the phase angle graph related to a second or third time constant, as shown in Figures 11 and 12. The inductive behavior is usually explained in terms of the relaxation phenomenon of reaction intermediates [26].

The reaction intermediates could be originated because the anodic dissolution of magnesium occurs together with a phenomenon called the negative difference effect (NDE). In the experimental tests, NDE effect is characterized by an unexpected increase of the cathodic hydrogen evolution reaction when the anodic over-potential is increased.

Song et al, 1997a; Song et al 1997b [23, 27] proposed a new mechanism for the occurrence of NDE. The authors explained that the formation of a partially protective layer of $Mg(OH)_2$ has an important effect in the corrosion behavior of magnesium. In the present work the presence of magnesium hydroxide in the corrosion products is confirmed by the structural characterization of corrosion products by XRD technique as shown in Figure 13.

Song et al, 1997a; Song et al 1997b considered the following reactions in their discussion of the NDE:

$2H^+ + 2e^- \rightarrow H_2$ (cathodic partial reaction) (2)

$2Mg \rightarrow 2Mg^+ + 2e^-$ (anodic partial reaction) (3)

$2Mg^+ + 2H_2O \rightarrow 2Mg^{2+} + 2OH^- + H_2$ (chemical reaction NDE) (4)

$2Mg + 2H^+ + 2H_2O \rightarrow 2Mg^{2+} + 2OH^- + 2H_2$ (overall reaction) (5)

$Mg^{2+} + 2OH^- \rightarrow Mg(OH)_2$ (corrosion product formation) (6)

The dissolution process mechanism depends on the rise of the film-free surface areas with increasing anodic potential on which the anodic and cathodic partial reactions shown in Equations 2 and 3, can take place more freely than on the surface coated by a film.

The chemical reaction NDE shown in equation 4 represents the chemical oxidation of Mg^{+} to Mg^{2+}. The overall reaction displayed in equation 5 is the result of the sum of equations 2, 3 and 4. Finally, equation 6 is the responsible for the formation of $Mg(OH)_2$ corrosion product.

For higher anodic overpotentials, the rate of the chemical reaction is raised due to the increased concentration of Mg+ produced by equation 3, and there is a drastic increase in the amount of hydrogen evolved, at localized sites.

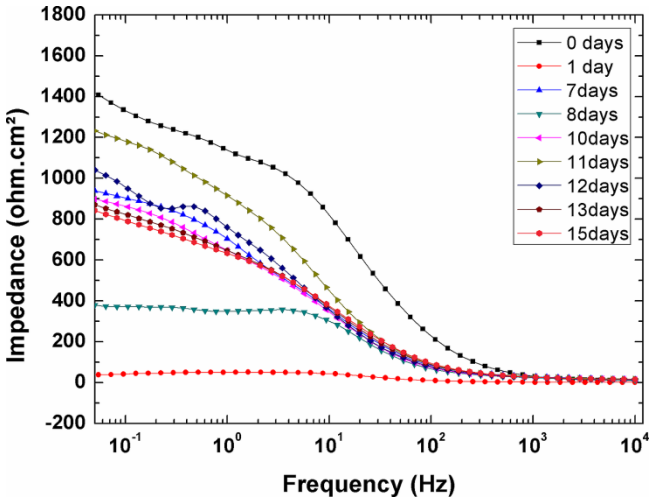

Figure 10. Bode diagrams for AlMgSi alloy corroded in the aqueous 3.5 % NaCl saline solution at room temperature.

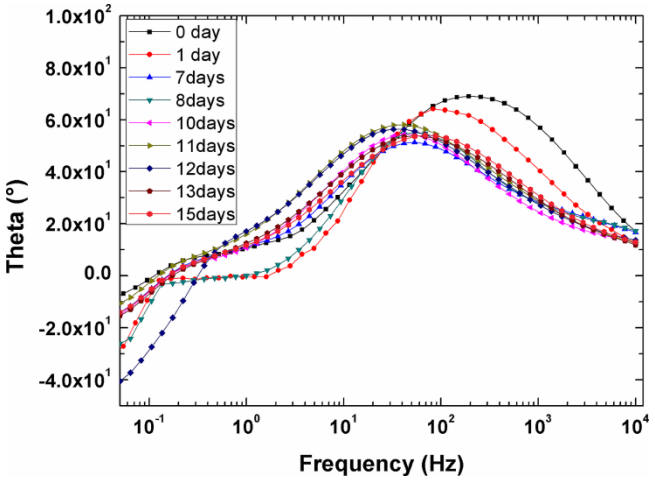

Figure 11. Bode phase diagrams for AlMgSi alloy corroded in the aqueous 3.5 % NaCl saline solution at room temperature.

As a matter of fact, there are several causes of inductive features in the electrode impedance. For example, when the potential shifts towards more negative values or time dependent change of the electrode interface induces the dissolution reaction, the inductive feature is expected. Regarding to Al-based alloys, Keddam et al. [26] and Chu-nan et al. [28] suggested that the inductive behavior is more likely promoted by the declination of the protectiveness of the oxide film. In the present work, a hydroxide film with partial protectiveness is formed as the corrosion products of the AlMgSi alloy over the surface, as revealed in the X-ray diffraction pattern shown in Figure 13. It is suggested that the inductive phenomenon, also is associated with the weakening of the effectiveness of this hydroxide film.

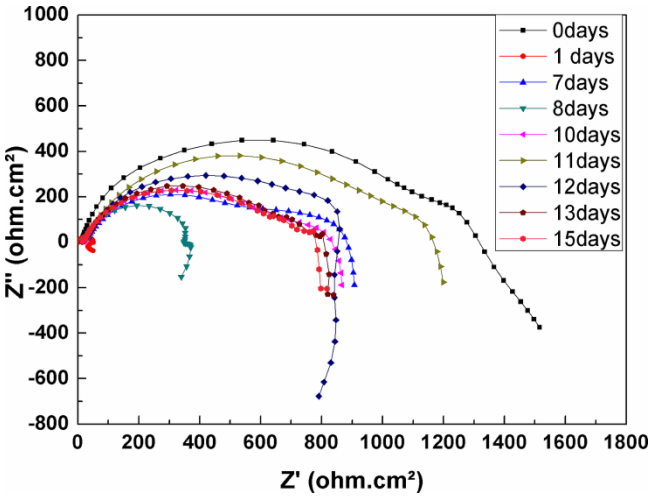

Figure 12. Nyquist diagrams for AlMgSi alloy corroded in the aqueous 3.5 % NaCl saline solution at room temperature.

3.8. Structural characterization of corrosion products by X-Ray Diffraction (XRD).

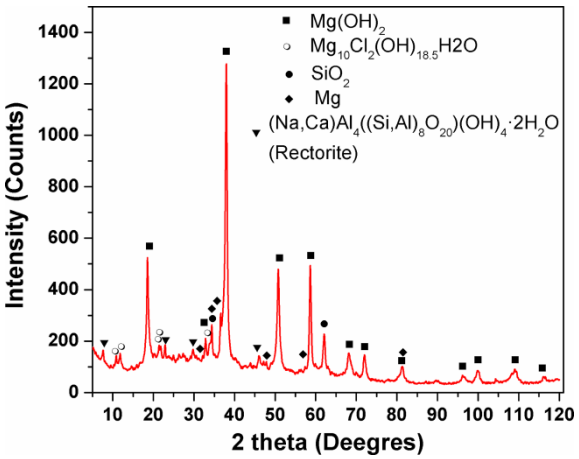

Figure 13. X-ray diffraction patterns of corrosion products of AlMgSi alloy after immersion during 20 days in 3.5 % NaCl saline solution.

Figure 13 shows the XRD profiles of corrosion products of AlMgSi alloy after exposure to 3.5 % NaCl saline solution. Diffraction peaks revealed the existence of the following phases: magnesium hydroxide (crystal system trigonal), hydrated magnesium chloride hydroxide, silicon dioxide, magnesium and Rectorite mineral (Crystal structure monoclinic). These results indicate preferential corrosion attack of Mg, this behavior being due to its high reactivity or low electrode potential as compared with the Aluminum electrode potential. Eliezer et al. [29] and Gutman 1994 [30] stated that the reactivity of Magnesium easily leads to corrosion even in the atmosphere.

The Mg detected in the diffractogram, displayed in figure 13, was formed according to equation (3), or could have also been detached from the interdendritic regions of AlMgSi alloy (see figure 1) and afterwards deposited in the corrosion products.

Is important to highlight that there were no evidence of corrosion products associated with aluminum in the X-ray profile, as the general reaction for corrosion of Al is represented in equation 7.

$$2Al + 3H_2O + \tfrac{3}{2}O_2 \rightarrow 2Al(OH)_3 \quad (7)$$

The SiO_2 phase which was revealed in the X-ray diffraction profile was formed by the reaction of silicon contained in the AlMgSi alloy and the H_2O of the solution according to the inverse reaction, shown in equation 8:

$$SiO_{2(s)} + 4H^+ + 4e^- \leftrightarrow Si_{(s)} + 2H_2O \quad (8)$$

Equation (8) is representative of the half-reaction reduction of silica. This half-reaction has a standard reduction potential, E° equal to -0.86 V.

The half-reduction reactions of aluminum and magnesium, together with their respective standard reduction potentials are shown in equations 9 and 10.

$$Mg^{2+} + 2e^- \leftrightarrow Mg \quad (-2.37\ V) \quad (9)$$

$$Al^{3+} + 3e^- \leftrightarrow Al \quad (-1.66\ V) \quad (10)$$

According to equations 9 and 10, the standard reduction potential of Mg^{2+} resulted to be the most negative, therefore, will be greater the tendency for the reverse reaction to occur, see equation 11.

$$Mg \rightarrow Mg^{2+} + 2e^- \quad (11)$$

Also, the fact that the standard reduction potential of the Mg^{2+} is the most negative, indicates that Mg is more reactive or less stable compared to Al or Si in the experimental arrangement under study. Therefore, according to the above explanation, the $Mg(OH)_2$ phase revealed in the diffraction profile of Figure 13, is present in a higher content.

Once formed the Mg^{2+} ion, it will react with OH^- to form Mg $(OH)_2$ according to equation 6. Also, when the Mg^{2+} ion chemically interacts with the OH^- and Cl^- ions, then the compound $(Mg_{10}Cl_2(OH)_{20})$ is formed according to the reaction shown in the equation 12:

$$10Mg^{2+} + 20(OH^-) + 2Cl^- \rightarrow Mg_{10}Cl_2(OH)_{20} \quad (12)$$

It is worth noticing that the Magnesium Chloride Hydroxide formed by equation 11 presents a slight difference of the content of OH ions as compared with the hydroxide $(Mg_{10}Cl_2(OH)_{18})$ revealed in the X-Ray diffraction pattern shown in figure 13. This difference in stochiometric is probably because this hydroxide compound can exist with a little deviation in its stochiometry.

The rectorite mineral could have been formed by a complex mixture of the hydrated oxides; besides, in the solution is present a ions cocktail of Na^+, Cl^- together with H^2O and Ca impurities, which justifies its presence in the other compounds that form the mineral.

4. CONCLUSIONS

As the concentration of Al, Mg and Si of ternary AlMgSi alloy exceeded the limit of solid solubility in Al then the Mg_2Si phase was precipitated together with a lower concentration of Si. Besides, pure magnesium was precipitated in the inter-dendritic regions of AlMgSi alloy.

The corrosion rate expressed in terms of corrosion current density of AlMgSi alloy resulted higher than that of pure Aluminum. This behavior could be due to the fact that the current density of Mg_2Si phase is bigger than the I_{corr} for pure Al.

In addition, the formation of the galvanic couple Al-Mg induced a shift of the corrosion rate towards higher values.

According to the structural characterization of corrosion products by X-ray diffraction technique, the following phases were revealed: Magnesium hydroxide, hydrated magnesium chloride hydroxide, Silicon dioxide, Magnesium and Rectorite mineral.

The variation trend of the E_{corr}, R_p and Z_t values with the exposure time, indicated that the hydroxide or oxide films formed over the surface of AlMgSi alloy were not fully protective.

According to electrochemical noise measurements the Al-based alloy experienced a localized type of corrosion at essentially all immersion days.

Quasi-inductive components in the low frequency region were observed in the AlMgSi alloy at all immersion times in the nyquist plot with a second peak in the phase angle graphic related to a second time constant. The inductive behavior is related with the relaxation phenomenon of reaction intermediates which are phases that form previously to the formation of the corrosion products composed mainly by hydroxides of magnesium.

ACKNOWLEDGEMENT
The authors express their gratitude to CONACyT and PROMEP for the financial support granted for the development of this research.

References

1. M. Okayasu, K. Ota, S. Takeuchi, H. Ohfuji, T. Shiraishi**,** *Mat. Sci. and Eng. A*, 592 (2010) 189-200.
2. T. Dursun, C Soutis, *Materials and Design,* 56 (2014) 862-871.
3. H. Ahlatci, E. Candan, H. Çimenoğlu, *Wear,* 257 (2004) 625–632.
4. A.Vieira, A. Pinto, L. Rocha, S. Mischler**,** *Electrochimica Acta,* 56 (2011) 3821–3828.
5. J. Xu, J. Zhang, S. Tang, W. Ren, *Mat. Sci. and Eng. A,* (2006) 433: 94-99.
6. G. Edwards, K. Stiller, G. Dunlop, M. Couper, *Acta Materialia*, 46 (1998) 3893-3904.
7. M. Murayama, K. Hono, W. Miao, D. Laughlin**,** *Metallurgical and Materials Transactions,* A 32 (2001) 239-246.
8. T. Sheppard, *Extrusion of aluminum alloys,* Kluwer Academic Publishers, Netherlands, Europe (2009).
9. D. G. Altenpohl**,** *Aluminum: Technology, Applications, and Environment: A profile of a modern Metal*. Minerals, Metals, and Materials Society, Warrendale Pennsylvania, USA (1998).
10. G. Svenningsen, J. Lein, A. Bjorgum, J. Nordlien, Y. Yu, K. Nisancioglu, *Corrosion Science*, 48 (2006) 226-242.

11. G. Svenningsen, M. Larsen, J. Nordlien, K. Nisancioglu**,** *Corrosion Science*, 48 1 (2006) 258-272.
12. J. Zahavi, J. Yahalom**,** *Journal of the Electrochemical Society*, 129 (1982) 1181-1185.
13. R. Ambat, A. Davenport, M. Scamans, A. Afseth, *Corrosion Science*, 48 (2006) 3455-3471.
14. J. Mol, B. Hinton, D. Van der Weijde, J. De Wit, S. Van der Zwaag, *Journal of Materials Science*, 35 (2000) 1629-1639.
15. V. Guillaumin, G. Mankowski, 2000**,** *Corrosion Science*, 42 (2000) 105-125.
16. C. Liao, R. Wei**,** *Electrochimica Acta*, 45 (1999) 881-888.
17. O. Lunder, J. Walmsley, P. Mack, K. Nisancioglu, *Corrosion Science*, 47 (2005) 1604-1624.
18. K. Mizuno, A. Nylund, I. Olefjord, *Corrosion Science*, 43 (2001) 381-396.
19. K. Yasakau, M. Zheludkevich, S. Lamaka, M. Ferreira, *Electrochimica Acta*, 52 (2007) 7651-7659.
20. R. Buchheit, *Journal of Electrochemistry Society*, 142 I11 (1995) 3994-3996.
21. L. E. Mondolfo, *Aluminium Alloys - Structure and Properties*, Butterworths, Belfast U.K. (1976).
22. F. Zeng, Z. Wei, J. Li, Ch. Li, X. Tan, Z. Zhang, Z. Zheng, *Transactions of Nonferrous Metals Society of China*, 21 I12 (2011) 2559-2567.
23. G. Song, A. Atrens, D. Stjohn, J Nairn, Y. Li, *Corrosion Science*, 39 (1997) 855-875.
24. G. Song, A. Atrens, *Advanced Engineering Materials*, 1 I1 (1999) 11-33.
25. Z. Rong-chang, Z. Jin, H. Wei-Jiu, W. Dietzel, K. Kainer, C. Blawert, K. Wei, *Trans. Nonferrous Met. Soc. China*, 16 (2006) 763-771.
26. M. Keddam, C. Kuntz, H. Takenouit, D. Schuster, D. Zuili, *Electrochimica Acta*, 42 (1997) 87-97.
27. G. Song, A. Atrens, D. Stjohn, X. Wu, J. Nairn, *Corrosion Science*, 39 (1997) 1981-2004.
28. C. Chu-nan, W. Jia, L. Hai-chao, *Journal of Chinese Society of Corrosion and Protection*, 9 4 (1989) 261-270.
29. A. Eliezer, E. Gutman, E. Abramov, E. Aghion, *Materials Science Forum*, 517528 (1998) 278-292.
30. E. M. Gutman, *Mechanochemistry of solid surface*, World Scientific Publishing, Singapore, ASIA (1994).